Failure Process Analysis of Landslide Triggered by Rainfall at Volcanic Area: Fangshan Landslide Case Study

Weiwei Gu, Zinan Li, Cheng Lin, Faming Zhang, Menglong Dong, Yukun Li, and Chang Liu

2022

water

MDPI

Article

Failure Process Analysis of Landslide Triggered by Rainfall at Volcanic Area: Fangshan Landslide Case Study

Weiwei Gu [1], Zinan Li [2,3,*], Cheng Lin [3], Faming Zhang [2], Menglong Dong [2], Yukun Li [2] and Chang Liu [2]

[1] China Coal Changjiang Ecological Environment Technology Co., Ltd., Nanjing 210046, China
[2] School of Earth Sciences and Engineering, Hohai University, Nanjing 211100, China
[3] Department of Civil Engineering, University of Victoria, 3800 Finnerty Road, Victoria, BC V8P 5C2, Canada
* Correspondence: lizinan@hhu.edu.cn

Abstract: The Fangshan landslide was a rainfall-induced landslide that occurred in a volcanic area in the Fangshan scenic spot, Nanjing, Jiangsu, China. On 25 October 2016, after approximately 10 days of continuous rainfall, a shallow landslide rapidly developed, which triggered slow movement of deep mudstone rock. According to the characteristics of the landslide body, measures such as anti-slide piles, anchor cables and drainage were used to reinforce the landslide. Active drainage measures included arranging plant growth zones at the trailing edge of the landslide, and passive drainage measures included arranging pumping wells at the trailing edge of the landslide. It is worth emphasizing that the Fangshan landslide was the first example of a landslide in Jiangsu Province, China that was treated by actively lowering the water pressure. After landslide treatment from 16 May 2017 to 21 January 2018, the Fangshan landslide tended to be stable. However, the stable landslide was reactivated by the rise in groundwater level caused by rainfall and pumping well damage and underwent accelerated downward sliding in July 2020. The Fangshan landslide has caused great damage to the roads and buildings of Fangshan scenic spot, with a direct loss of RMB 6 million and an indirect loss of RMB 95 million. This article discusses the development process of the shallow soil landslide and the underlying deep mudstone rock landslide. The influence of groundwater level variation on the deformation of the shallow soil landslide and deep mudstone rock landslide of the Fangshan landslide are also discussed.

Keywords: sequential sliding landslide; volcanic area; permeability; ground water level variation; long-term deep and surface displacement monitoring

Citation: Gu, W.; Li, Z.; Lin, C.; Zhang, F.; Dong, M.; Li, Y.; Liu, C. Failure Process Analysis of Landslide Triggered by Rainfall at Volcanic Area: Fangshan Landslide Case Study. *Water* **2022**, *14*, 4059. https://doi.org/10.3390/w14244059

Academic Editors: Xingwei Ren, Zili Dai and Fangzhou Liu

Received: 26 September 2022
Accepted: 11 November 2022
Published: 12 December 2022

1. Introduction

Rainfall is a major factor in inducing landslides. When the duration and intensity of rainfall exceed a certain threshold, the probability of landslide failure increases significantly [1–7]. To explore the impact of rainfall on the specific landslide failure process, it is particularly important to identify its specific hydrogeological conditions. The rise of aquifer water level will lead to pore water pressure changes, accelerating the movement of landslides, and applying drainage measures to decrease the water level of aquifers will effectively improve the long-term stability of landslides [8–15]. Most cases that have discussed the triggering factors of the landslide occurring in volcanic areas proposed that the high permeability of the layer formed by the accumulation of weathered volcanic debris was the main reason for the landslide [2,6,7,11]. A previous study on the Fangshan landslide discussed the triggering factor and proposed that a low-permeability layer can restrict the activity of the lower aquifer and that would lead to a failure of landslide [16]. However, the former study ignored the occurrence of deep landslides triggered by the movement of overlaying shallow landslides, and discussed only one class of landslides. Combining long-term monitoring data, monitored water level variation, and more detailed survey data, which was not discussed in the previous study, we analysed the formation process of

deep rock landslides, and discuss the different effects of water level variation on this type of sequential sliding landslide. According to the groundwater level monitoring data of 13 pumping wells during the Fangshan landslide reactivation period, we discuss the failure of the Fangshan landslide again. Moreover, according to the problems encountered in the treatment of the Fangshan landslide, suggestions are proposed to deal with the special type of landslide which occurs in volcanic areas.

The Fangshan landslide is a rainfall-induced landslide in a volcanic area located in the Fangshan scenic district, Nanjing City, Jiangsu, China. Fangshan Mountain is an extinct volcano that erupted 5 million years ago and is famous for its unique natural landscape and long cultural history. Additionally, it is the only volcanic landform area in East China. There are more than 100 relics and cultural sites remaining at Fangshan scenic district, such as the Dinglin Temple Pagoda, Dongxuan temple, Sun Quan Dianjiang platform and Wang Seng's tomb, which are important parts of Nanjing's culture. Since several different kinds of extrusive rock are well preserved in the Fangshan scenic district, it is also considered representative of volcanic areas, which has important scientific significance and value. The Fangshan landslide covers an area of 101,932 m^2, with a length of 450 m and width of 280 m. After the occurrence of the Fangshan landslide, various roads, bridges, cables, retaining walls, and drainage ditches, a grass skiing ground and other public facilities in the scenic area were damaged. Additionally, the road up to the mountain from the eastern entrance of the scenic area was completely blocked, with direct loss of RMB 6 million and indirect loss of RMB 95 million.

1.1. Topography and Geologic Setting

The Fangshan landslide (118°52′44″ E, 31°53′58″ N) is located northeast of Fangshan Mountain (Figure 1). The landform on Fangshan Mountain is denuded monadnock, with an altitude of 208 m. The topography in the mountain area is characterized by a steep top part, which includes the crater, and more gently sloping in the middle and lower parts, which are surrounded by plains. The lithologic distribution of Fangshan Mountain is as follows: the crater is diabase, around the crater is basalt, the middle and lower parts of the mountain are tertiary Dongxuanguan Formation mudstone, and the toe of the mountain is widely distributed tertiary Chishan Formation argillaceous sandstone.

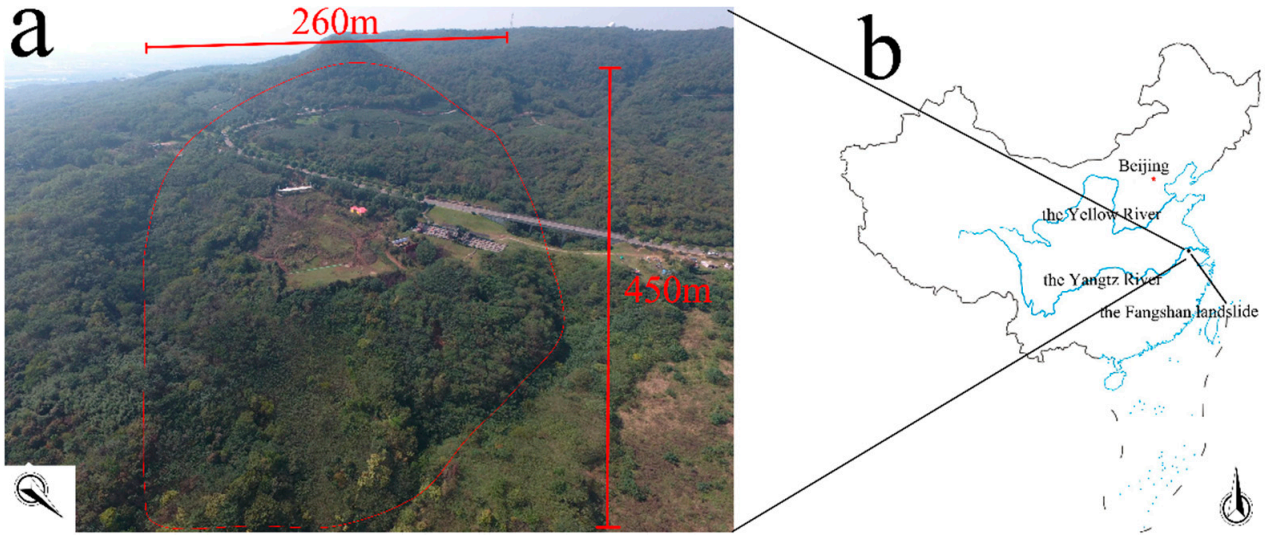

Figure 1. (**a**) Aerial image of the 3 November 2016, Fangshan landslide; (**b**) location of Fangshan landslide. The base map of China is from the standard map, review number: GS (2016) 1549.

1.2. Climate and Rainfall

Impacted by the 2015–2016 El Niño event, heavy precipitation occurred many times in Nanjing in 2016. The precipitation from 30 June 2016 to 8 July 2016 was in total 498 mm [17], exceeding the historical record. Figure 2 shows the cumulative rainfall in Nanjing from 11 June 2017 to 12 December 2020.

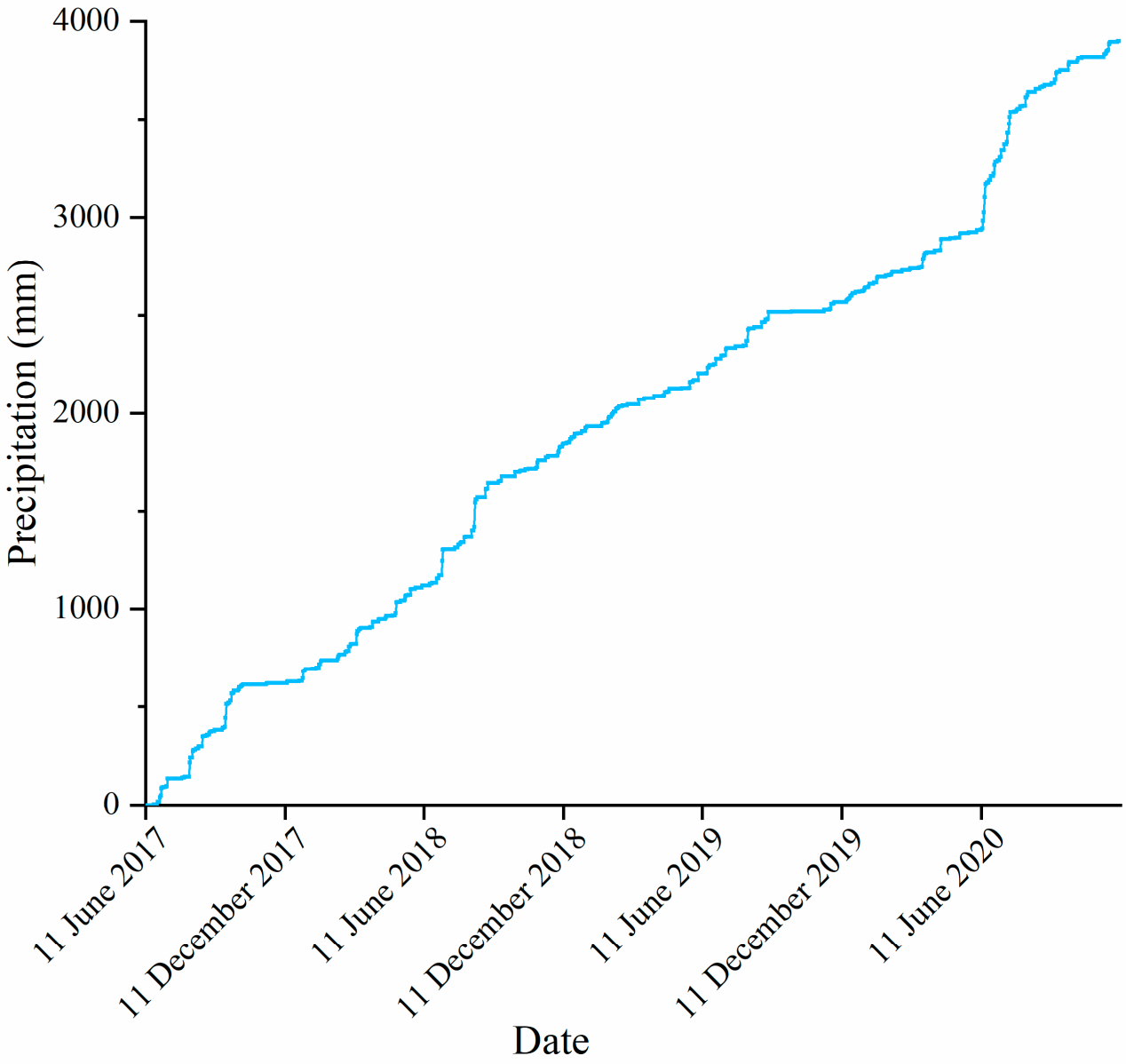

Figure 2. Cumulative rainfall in Nanjing from 11 June 2017 to 12 December 2020.

1.3. Overview of the Landslide

The Fangshan landslide is a thrust-type with both shallow soil and deep rock landslide failure types. It is approximately 450 m long, 280 m wide, and 101,932 m^2 in area and is triggered by rainfall in the volcanic area. The timeline (Figure 3) of the development of the Fangshan landslide lasted four years, which could be divided into five stages. In stage 1, the shallow soil landslide occurred. In stage 2, the deep mudstone rock landslide occurred. In stage 3, the Fangshan landslide was reinforced by the Fangshan Scenic Area Administration. In stage 4, the Fangshan landslide remained stable after reinforcement. In stage 5, the Fangshan landslide reactivated. These stages are discussed in detail.

Stage 1: On 15 July 2016, due to the impact of unusual rainstorms in Nanjing, cracks with widths of 3–20 mm were observed in the scenic road in the middle of the landslide. Since then, the landslide area has been in a slow deformation stage. On 16 September 2016, the Fangshan landslide developed in the middle of the mountain, and there was an obvious sliding trace on the surface. The trailing edge of the landslide formed a scarp 0.5 m high (Figure 4a). On 25 October 2016, due to continuous rainfall over approximately 10 days, the shallow soil landslide failed as a whole, and the front edge of the landslide extended to the foot of the mountain, which posed a serious threat to the main road and bridge. Stage 2: According to the monitoring data from five deep displacement monitoring points (P1–P6, whose positions are shown in Figure 5) before treatment from 10 November 2016 to 12 April 2017, the deep horizontal displacement of the Fangshan landslide continued to increase. According to the deep displacement monitoring data, a new extreme value point appeared in the monitoring curve P5 and P6, which indicated the deep mudstone rock landslide was gradually forming. Stage 3: From 16 May 2017 to 21 January 2018, the Fangshan Scenic Area Administration reinforced the landslide (the reinforcement measures are shown in Figure 6) and installed 15 surface monitoring points (D1–D15) and six deep horizontal displacement monitoring points (CX1–CX6) on 11 June 2017 for long-term monitoring. Stage 4: The Fangshan landslide remained stable after treatment. Stage 5: In early July 2020, with pumping equipment damage, the stable landslide was reactivated by the rise in groundwater level and exhibited accelerated downward sliding. From 18 July 2020 to 6 August 2020, the groundwater level of 13 pumping wells was recorded. On 29 July 2020, the groundwater level of the landslide returned to normal level, and the landslide tended to be stable again.

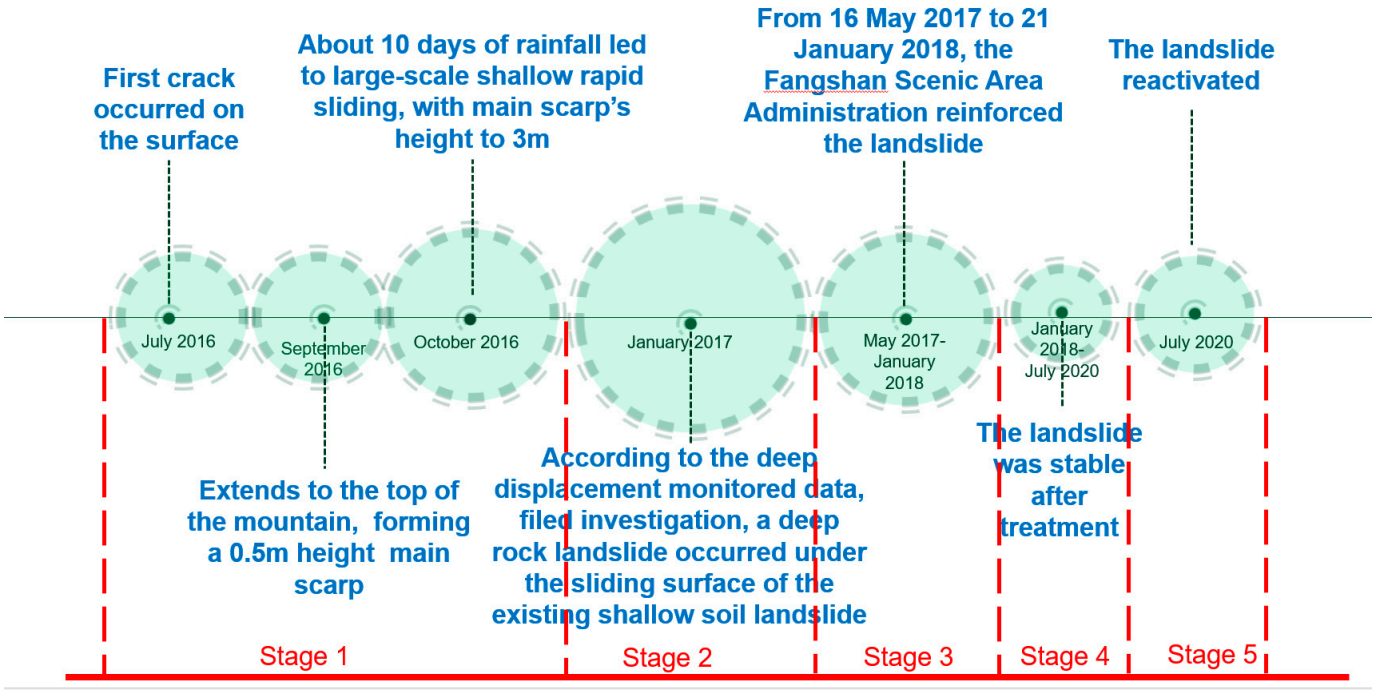

Figure 3. Timeline of the development of the Fangshan landslide.

Figure 4. (**a**) Scarp on the trailing edge of landslide, photographed 23 September 2016; (**b**) scarp on the trailing edge of landslide, photographed 3 November 2016; (**c**) broken mountain road; (**d**) toppled trees; (**e**) cracks on Dlinglin Road; (**f**) deformation of retaining wall; (**g**) groove on the northwest side of landslide; (**h**) subsidence of groove [16]; (**i**) cracks on Zulong Road; (**k**) cracks on Dinglin Road; (**l**) front shear outlet; (**m**) groundwater flowing out of the surface, their positions are shown in Figure 5.

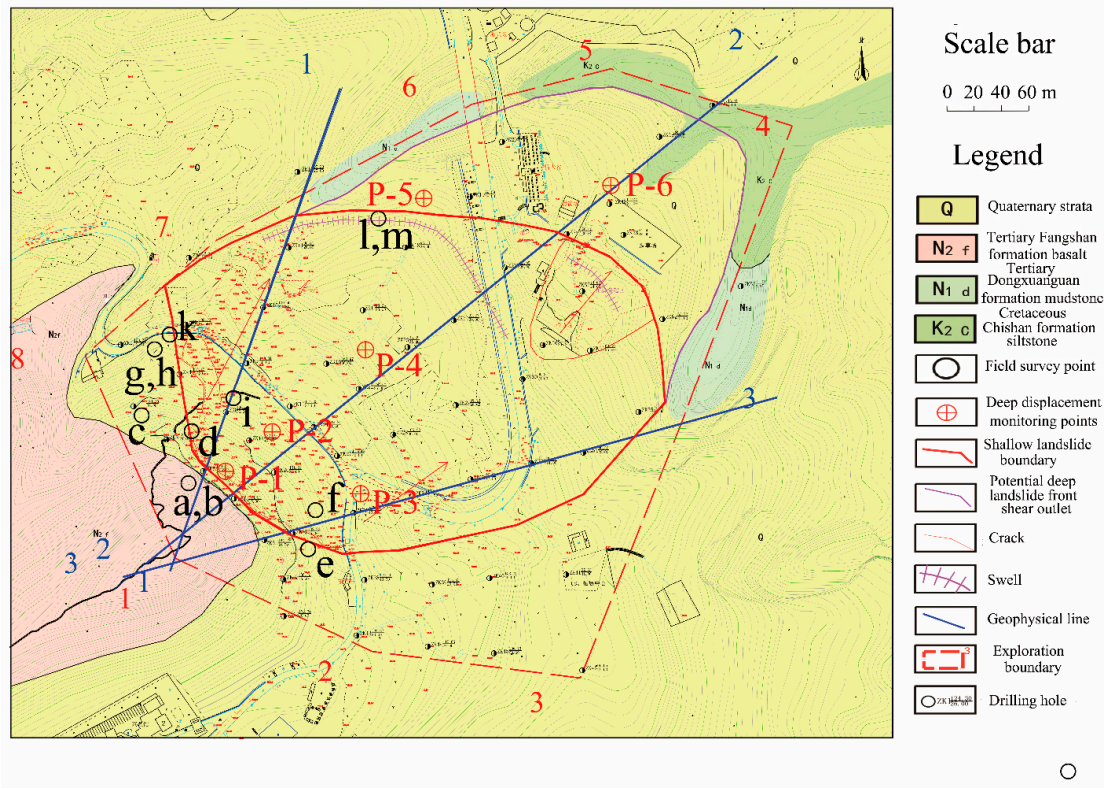

Figure 5. Investigation results of the Fangshan landslide, which shows the distribution of layers on the surface ground, the results of the field surface survey, the location of P1–P6 deep monitoring points and the geophysical line. Numbers 1–8 indicated the field investigation area.

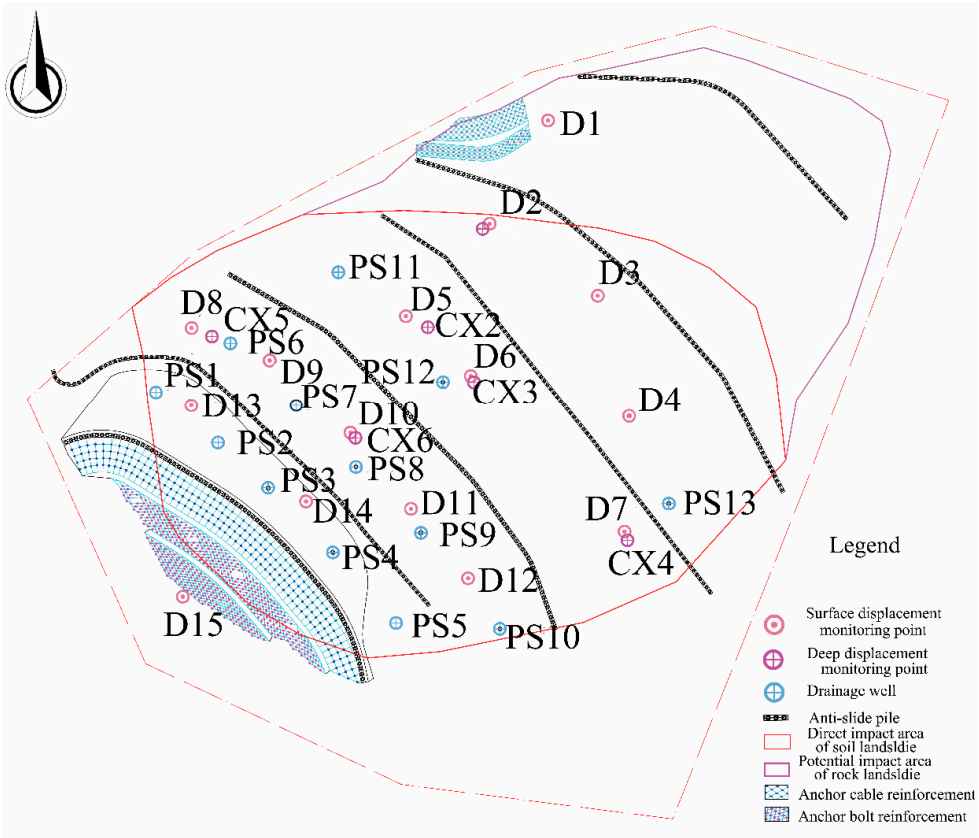

Figure 6. Treatment of the Fangshan landslide and location of monitoring points.

2. Methods

We mapped the extent and features of the Fangshan landslide using topographic data and images from the following sources: The map was drawn using total station, with 0.15 km^2 measurement range. Drilling holes and geophysical sections were measured by the high-density electrical method and audio-frequency magnetotelluric method was arranged to examine the features of the Fangshan landslide. Permeability tests, six deep displacement monitoring points before treatment, 15 landslide surface monitoring points and six deep displacement monitoring points after treatment were arranged to explore the failure mechanism and process of the landslide. Combined with the daily rainfall data from 11 June 2017 to 12 December 2020, the correlation between landslide deformation and rainfall was analyzed. Based on the analysis of the geological structure and deformation stage of the landslide, according to the groundwater level monitoring data of 13 pumping wells (SP1-SP13, from 18 July 2020 to 6 August 2020), the different effects of groundwater level variations on shallow soil landslide and deep mudstone rock landslide were examined. We also used the finite difference method to analyze the stress variation on the deep sliding surface position, which would help us better understand the failure process.

3. Results and Discussion

3.1. Geological Features

The geological features of the landslide were obtained from drilling holes (Figure 7), field surveys, and geophysical sections, whose locations are shown in Figure 5. Figures 8–10 show the apparent resistivity maps of section 1-1, section 2-2, and section 3-3, measured by the high-density electrical method and audio-frequency magnetotelluric method. According to the geological profiles (Figure 11) obtained from the geophysical prospecting and borehole measurements, from surface to underground, the lithologies of the landslide were as follows:

(**a**) Drilling (**b**) Drilling

Figure 7. Drilling construction site.

(1) Clay: greyish yellow, plastic to hard plastic, high strength. (2) Gravelly soil: grey to greyish yellow heterogeneous clay, distributed within a 0.05–1 m radius of the porous massive basalt and dense massive basalt, accounting for 50–80% of the total volume. (3) Clay: yellow, hard, plastic, high-strength, locally silty clay. (4) Strongly weathered basalt (sandy): greyish black, strongly weathered, sandy, with a small amount of gravel, and friable. (5) Strongly weathered basalt (gravelly): greyish black, developed

weathering fractures, gravelly, and locally sandy. (6) Strongly weathered mudstone: yellow to greyish white, strongly weathered, friable, expansive and easy to soften after soaking, with a high content of kaolin locally. (7) Strongly weathered glutenite: variegated, strongly weathered, friable, and less than 1.5 m thick; this is an interlayer in the strongly weathered mudstone. (8) Moderately weathered mudstone: greyish yellow, not friable, but with water softening properties.

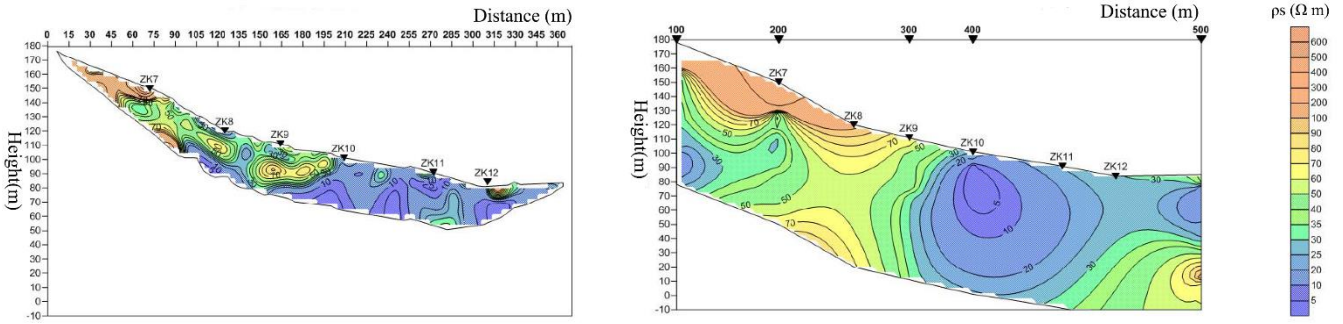

(**a**) Mapped by high-density electrical method (**b**) Mapped by audio-frequency magnetotelluric method

Figure 8. Geophysical section of 1−1.

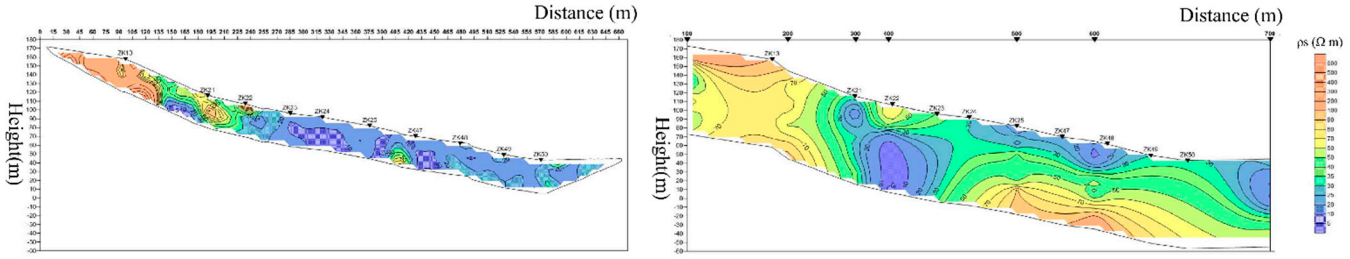

(**a**) Mapped by high-density electrical method (**b**) Mapped by audio-frequency magnetotelluric method

Figure 9. Geophysical section of 2−2.

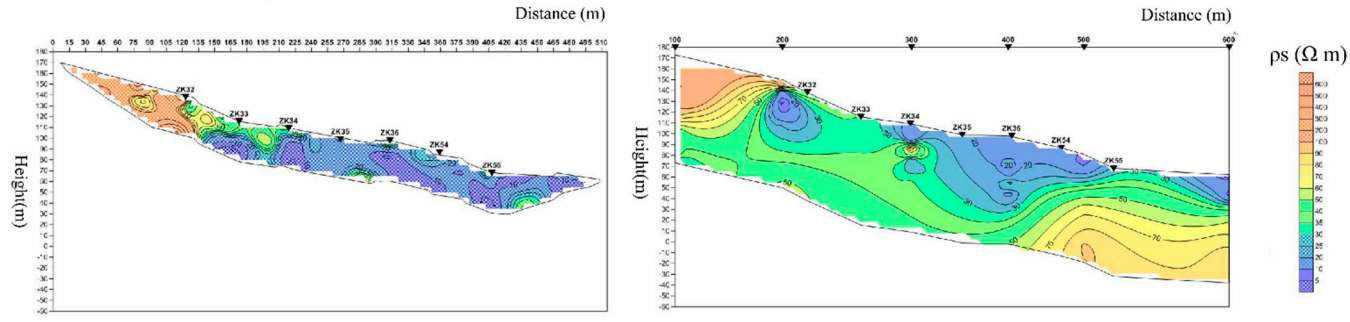

(**a**) Mapped by high-density electrical method (**b**) Mapped by audio-frequency magnetotelluric method

Figure 10. Geophysical section of 3−3.

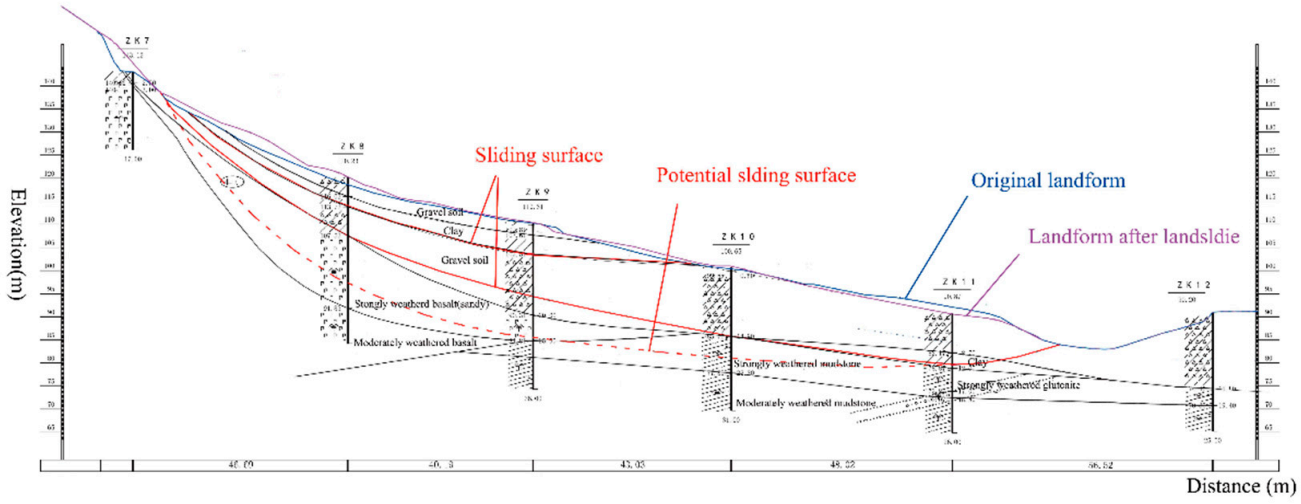

(**a**) Section 1–1

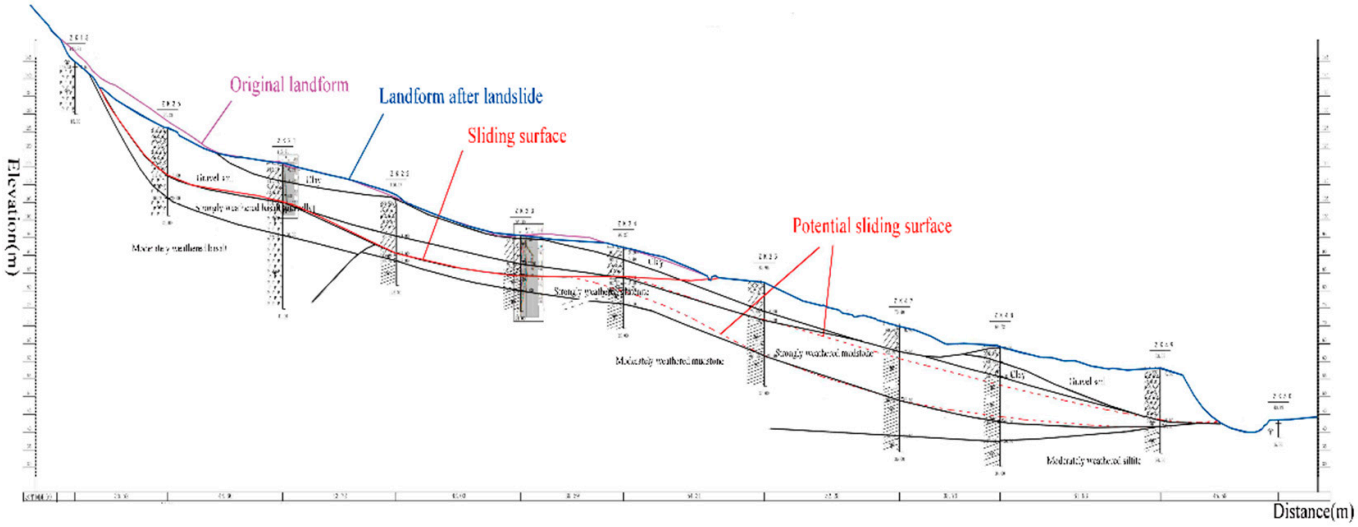

(**b**) Section 2–2

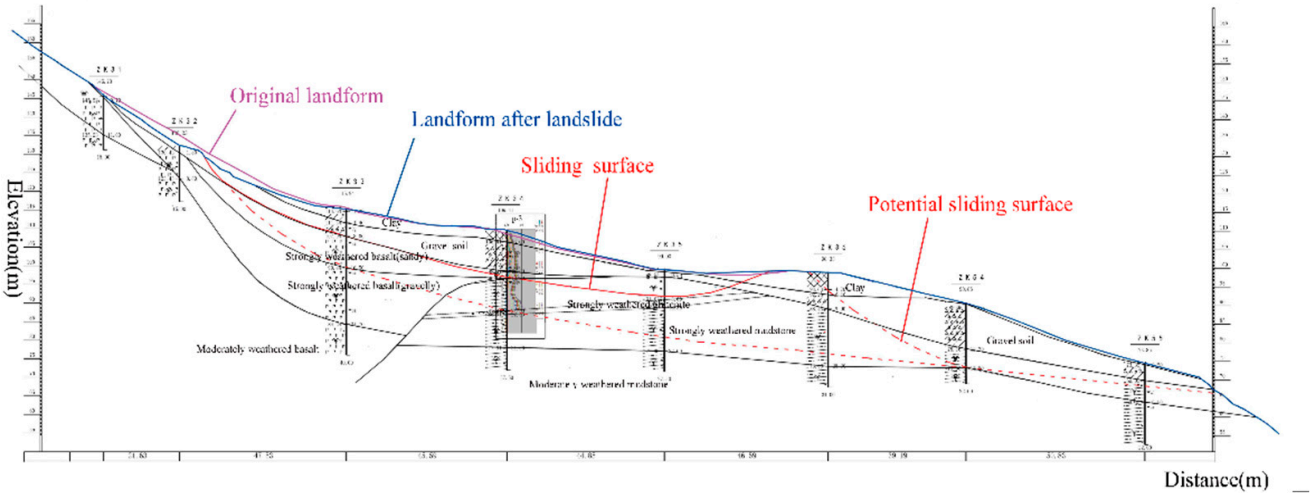

(**c**) Section 3–3

Figure 11. Geophysical profiles of the Fangshan landslide.

3.2. Hydrogeological Conditions

Surface floods often occurred in the study area during the rainy season (Figure 12), and it is meaningful to investigate the hydrogeological conditions of each layer to examine the failure process of such rainfall-induced landslides that occur in volcanic areas. The samples for variable head permeability test were sampled perpendicular to the soil sample level, some from drilling holes (Figure 7), some from the same type of layer exposed. Combined with experience from surrounding projects and previous studies [16] and water pressure testing drilling holes, Table 1 shows the results of permeability coefficients used in the design of landslide treatments, which showed that the hydraulic conductivity of each rock layer in the study area varied greatly, up to four orders of magnitude. Specifically, gravelly soil and strongly weathered basalt (sandy and gravelly) formed by the volcanic eruption have high permeability, and clay and mudstone formed by natural deposition have poor permeability, which corresponds to aquifers and relative aquicludes. From surface to underground, the layers include the following: (1) Clay: low permeability, relative aquiclude; (2) Gravelly soil: high permeability, aquifer. (3) Clay: low permeability, relative aquiclude. (4) Strongly weathered basalt (sandy): high permeability, aquifer. (5) Strongly weathered basalt (gravelly): high permeability, aquifer. (6) Strongly weathered mudstone: low permeability, relative aquiclude. (7) Strongly weathered glutenite: high permeability, aquifer. (8) Moderately weathered mudstone: low permeability, relative aquiclude.

Figure 12. (**a**–**c**) were surface floods taken during the rainy season.

Table 1. Permeability of each layer.

Layer	Vertical Hydraulic Conductivity Kv (cm/s)	Horizontal Hydraulic Conductivity Kh (cm/s)
Clay	2.8×10^{-7}	3.0×10^{-7}
Gravelly soil	2×10^{-3}	5.0×10^{-3}
Clay	2.8×10^{-7}	3.0×10^{-7}
Strongly weathered basalt (sandy)	3×10^{-5}	4.0×10^{-5}
Strongly weathered basalt (gravelly)	3×10^{-3}	4.0×10^{-3}
Strongly weathered mudstone	3×10^{-7}	3.0×10^{-7}
Strongly weathered glutenite	2×10^{-3}	5.0×10^{-3}
Moderately weathered mudstone	2×10^{-7}	2.0×10^{-7}

3.3. Main Features of Fangshan Landslides

Figure 5 shows the field investigation results after the occurrence of the landslide. The whole landslide had a narrow trailing edge and a wide leading edge. The sliding direction of the landslide was 10–75°, radiating outward. The sliding direction of the central axis of the landslide was approximately 40°. The landslide material, structure and borehole data show that the Fangshan landslide was composed of two parts: one was the shallow soil landslide, caused by rainfall and seepage, and the other was the deep creep mudstone low-angle rock landslide, caused by the failure of the shallow surface soil landslide. Supporting evidence is discussed in detail in Section 3.4, and the reason is discussed in Sections 3.6 and 3.7. The field investigation reports and the monitoring data of five deep displacement monitoring points (P1–P5) before treatment showed that the deep rock landslide was in the continuous deformation stage after the overall instability of the shallow soil landslide on 25 October 2016. To facilitate analysis, the landslide area was divided into two regions: the direct impact area of the shallow soil landslide (region I) and the potential impact area of the deep rock landslide (region II). The investigation of the surface damage was mainly concentrated in region I, and the investigation of region II was mainly deduced by deep displacement monitoring point and drilling data.

The boundary of region I is clear. At the trailing edge, a 0.5 m scarp was found on 23 September 2016, and the scarp height increased to 3.5 m (Figure 4b) after the shallow soil landslide formed. The mountain road fractured (Figure 4c), and the mountain trees toppled (Figure 4d). On the southeast side, a large number of tensile and shear cracks occurred in Dinglin Road. The maximum height difference of the road is 1.5 m (Figure 4e), and the retaining wall on the side of the road was uplifted by extrusion (Figure 4f). On the northwest side, a groove (Figure 4g) with a width of approximately 20 m formed, and the subsidence depth was 2 m (Figure 4h). In the middle of region I, cracks and deformation were observed in many places along Zulong Road (Figure 4i) and Dinglin Road (Figure 4k). At the leading edge of region I, several front shear exits were observed, accompanied by soil and road uplift (0.3–1.2 m), and a large number of swelling cracks were observed (Figure 4i). The soil at the leading edge was saturated, and groundwater flowed on the surface (Figure 4m). According to the geophysical profile (Figures 8–10) and the data from the deep displacement monitoring points of the landslide before treatment (P1–P6), it was concluded that the sliding surface of the shallow surface soil landslide was mainly developed in the layer of gravelly soil or at the interface between the gravelly soil and strongly weathered mudstone, at a depth of 8–15 m. The sliding surface of the deep mudstone rock landslide was mainly developed at the interface between the strongly weathered mudstone and moderately weathered mudstone or in the layer of strongly weathered glutenite, which is an interlayer of the strongly weathered mudstone.

3.4. The Development Process of Deep Mudstone Rock Landslide

Figure 13 shows the deep monitoring data of P1–P6 from 10 November 2016 to 12 April 2017 (stage 2). The first large deformation of each deep displacement monitoring point appeared on P4, with its pipe of monitoring broken on 26 November 2016. And then, P1 and P2 monitoring points appeared largely deformed, with their monitoring pipes broken on 6 January 2016. Before the broken pipes of P1, we can clearly see a sharp increase appeared on 16 December 2016, which did not appear in other deep monitoring points at that time, combined with their location, the start of the exciting soil landslide was from the middle of the landslide, and gradually formed to the trailing edge of the landslide. Moreover, according to P5 and P6, which are located in region II, we can conclude that before 26 November 2016, the maximum displacement depth of point P5 was 12 m, and the maximum displacement depth of point P6 was 11 m. However, due to the continuous movement of the existing landslide and the influence of factors such as rainfall, under this geological structure type, the sliding depth migrated deeply. After 26 November 2016, at a depth of 21 m at point P5 and a depth of 20 m at point P6, a new maximum extreme value point of monitoring displacement curve appeared. As of 12 April 2017, the value of the

new maximum extreme value points exceeded or matched the displacement value of the previous maximum extreme point. That being said, the new maximum extreme value at the deeper depth of P5 and P6 appeared after the shallow landslide, which showed that after the apparent sliding of P1, P2, P3, and P4, the deep sliding points of P5 at depth of 21 m and P6 at depth of 20 m began to develop. This indicates that the shallow soil landslides led to the formation of deep rock landslides.

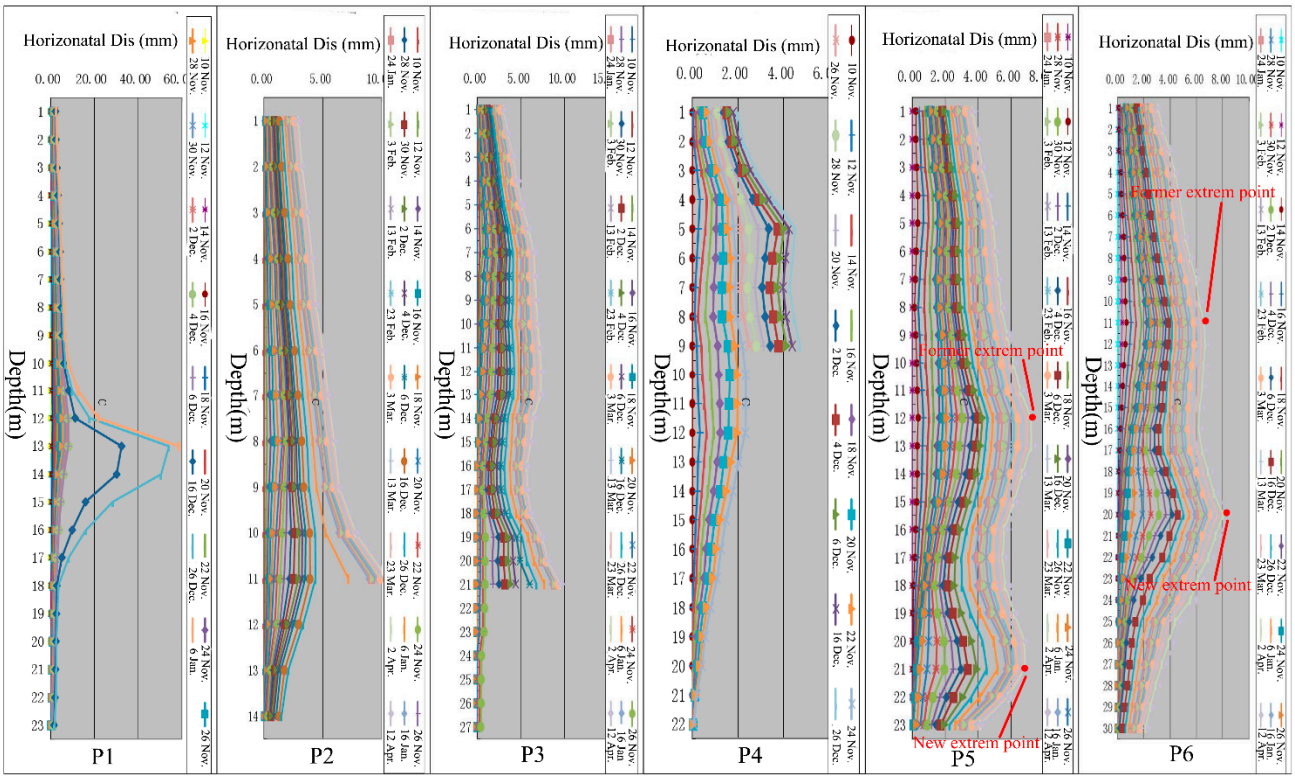

Figure 13. Monitoring of deep horizontal displacement before landslide treatment, from 10 November 2016 to 12 April 2017.

3.5. Analysis of Long-Term Displacement Deformation after Landslide Treatment

After the overall sliding of the shallow soil landslide on 25 October 2016, the treatment of the Fangshan landslide continued from 16 May 2017 to 21 January 2018, and the displacement of the Fangshan landslide was monitored from 11 June 2017 to 12 December 2020 (stage 3, stage 4 and stage 5), from 15 surface monitoring points and six deep horizontal displacement points (CX1–CX6), whose positions are shown in Figure 6. The treatment mainly included the following three measures (Figure 6): (1) Six rows (A, B, C, D, E, and F) of anti-slide piles were installed to prevent sliding. They were embedded in the weathered rock 4–5 m deep, with a spacing of 3 m along each row (the pile diameter of rows B, D, and E was 1.8 m, and the pile diameter of rows A and C was 1.5 m). (2) Slope cutting at the trailing edge of the landslide was performed, and anchor bolt and anchor cable reinforcements were added. Plant growth zones were also arranged at the trailing of the landslide after treatment. (3) A groundwater drainage system (13 pumping wells) was set up to reduce the groundwater level during construction and start drainage when the groundwater level exceeded the warning level after treatment.

Figure 14 shows the cumulative vertical displacement monitoring data of the 15 surface displacement monitoring points from 11 June 2017 to 12 December 2020. Figure 15 shows the cumulative monitoring data of six deep horizontal displacement monitoring points of the Fangshan landslide from 11 June 2017 to 12 December 2020. Figure 16 shows the details of the maximum displacement depth of each deep horizontal displacement monitoring point (CX1–CX6). Considering the surface displacement monitoring data and deep dis-

placement monitoring data of the landslide together, it was concluded that the landslide deformation trend during the period from 11 June 2017 to 12 December 2020, corresponding to the three periods previously divided: (1) Stage 3 (11 June 2016 to 21 January 2018) was the continuous sliding stage of the landslide, when the whole landslide slid outward at a relatively high rate. (2) Stage 4 (21 January 2018 to 2 July 2020), the landslide was basically stable. (3) Stage 5 (from 2 July 2020 to 12 December 2020), the landslide reactivated, and the whole landslide slid outward at a relatively low rate and eventually became stable. In stage 3, the monitoring curves of surface displacement monitors D5, D6, D7, D8, D10 and D11 and deep displacement monitors CX2, CX3, CX4 and CX5, whose displacements were relatively large, all exhibited obvious rebounds. The rebound occurred because during this period, the anti-slide piles were installed, and the downward-moving sliding body was blocked by the anti-slide piles, resulting in a small amount of uplift. The start of stage 5 was consistent with the time when the drainage well became damaged in early July 2020. Under the influence of continuous rainfall, the rise in groundwater level exceeded the control value because of the damage to the drainage wells, and the landslide began to slide outward again. Figure 17 shows the variation in groundwater level from 18 July 2020 to 9 August 2020. Compared with Figure 16, Figure 17 shows that when the water level of SP4 dropped from 105.7 m on 18 July 2020 to 99.534 m on 6 August 2020, the deep horizontal displacement of the landslide tended to be stable. Combined with the previous survey information, when the water level of the observation well exceeded the normal value, the existing water level was higher than the existing sliding surface position. It appeared that the rise in groundwater level caused by rainfall was the main factor leading to the reactivation of the Fangshan landslide.

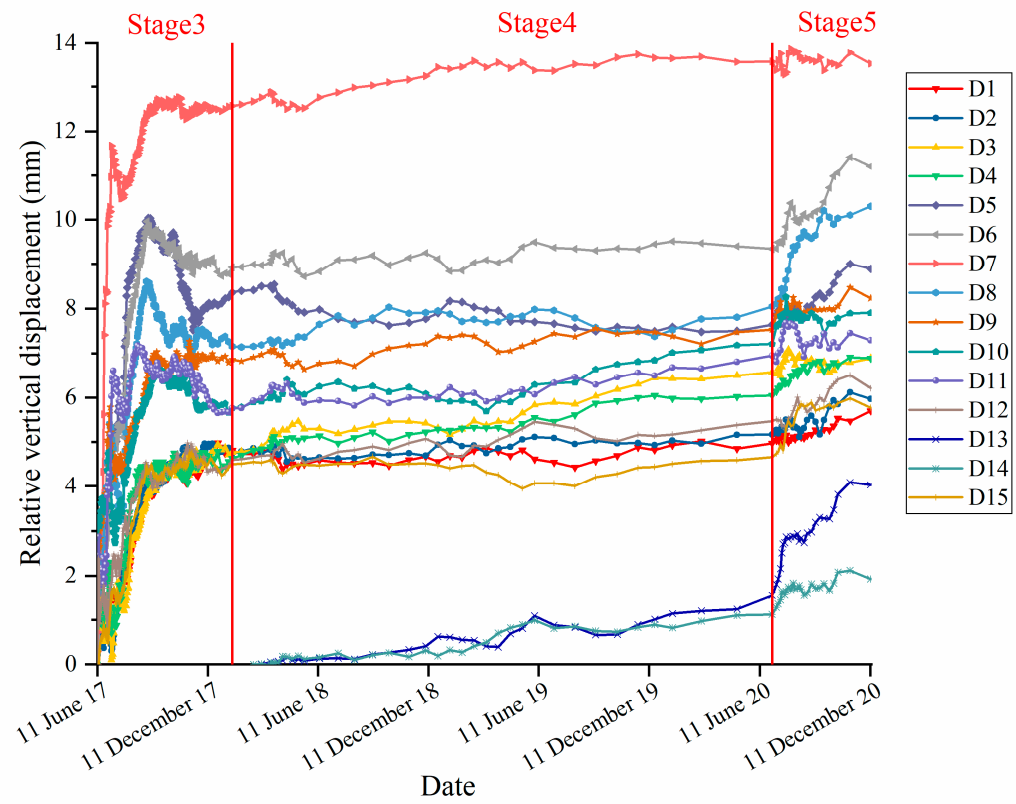

Figure 14. Cumulative vertical displacement monitoring data of 15 surface displacement monitoring points from 11 June 2017 to 12 December 2020. Their positions are shown in Figure 6.

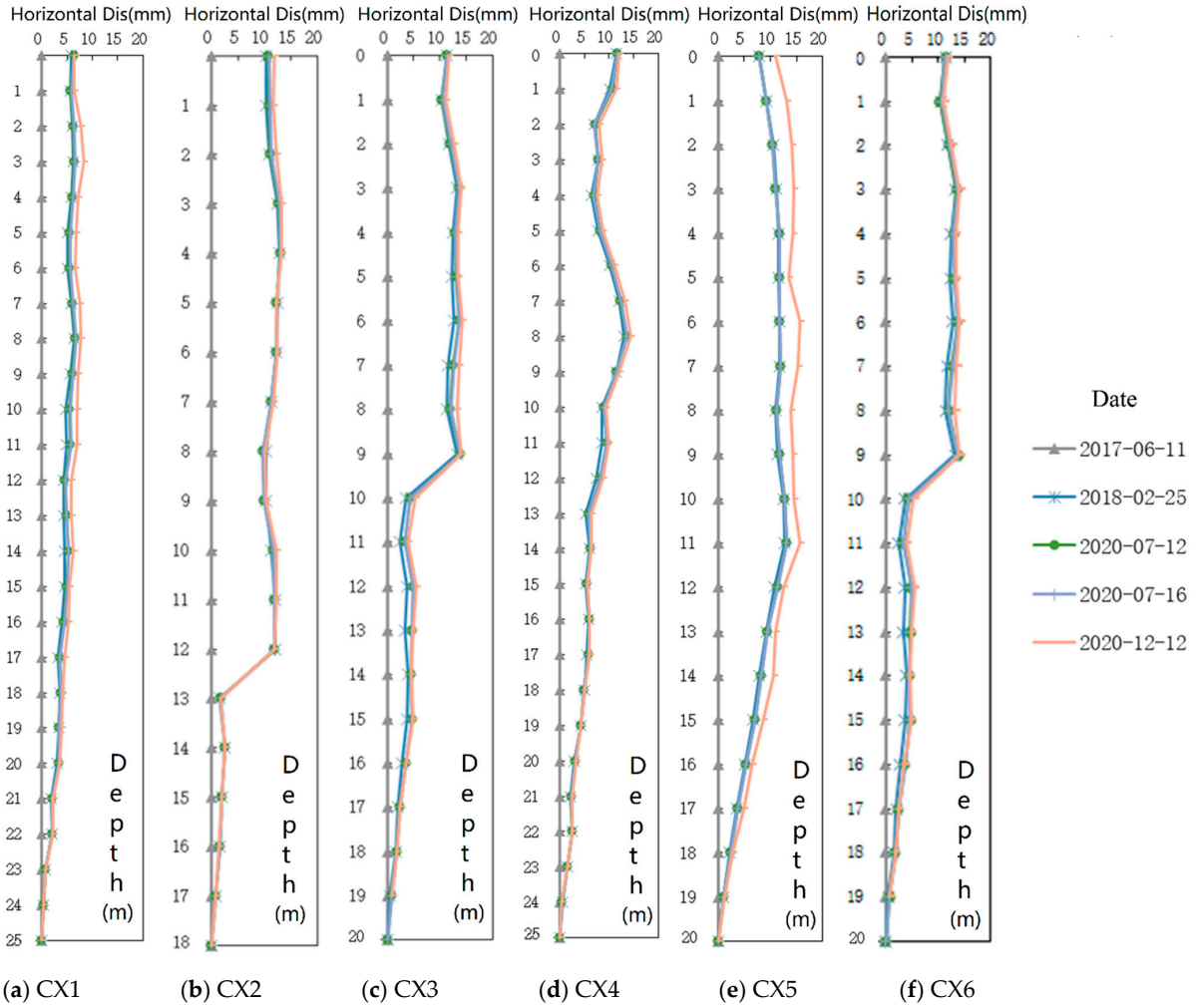

Figure 15. Cumulative monitoring data of six deep horizontal displacement monitoring points of Fangshan landslide from 11 June 2017 to 12 December 2020. Their positions are shown in Figure 6.

Since there were no long-term groundwater level monitoring data collected, to further explore the correlation between the rainfall and landslide displacement, according to the displacement change trend of the landslide and the distribution of the monitoring points, the surface displacement monitoring point D6 and deep displacement monitoring point CX3, which indicated relatively large displacements and were located in the middle of the landslide, and the surface displacement monitoring point D2 and deep displacement monitoring point CX1, which indicated relatively small displacements and were located in the front of the landslide, were selected for correlation analysis with the cumulative rainfall from 11 June 2017 to 12 December 2020. Because the changes in surface displacement and deep horizontal displacement were caused by the movement of the landslide, the cumulative incremental displacement was calculated by taking the absolute increment value in the correlation analysis. Considering the trend of deformation and the frequency of monitoring, the displacement of the missing data was determined by linear interpolation. Due to the seasonal changes in rainfall, the monthly displacement and the cumulative change in rainfall were selected to calculate the correlation between the monthly changes in rainfall and displacement and the percentage of monthly rainfall and displacement of the total change from 11 June 2017 to 12 December 2020. According to the calculation results in Figure 18, although the total displacement of the landslide had obvious differences among stage 3, stage 4 and stage 5, the deformation trend always maintained a high correlation with rainfall variation.

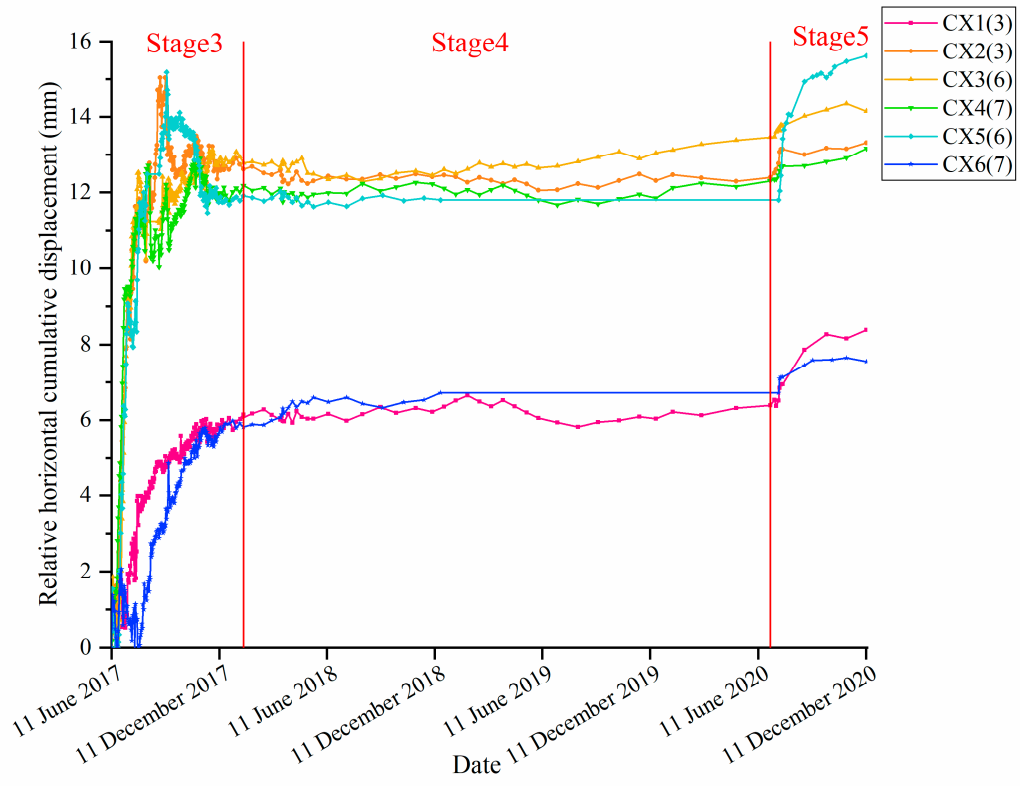

Figure 16. Detailed horizontal displacement deformation data of the maximum displacement depth of each deep horizontal displacement monitoring point. (Since the displacement values of CX5 and CX6 monitoring points from 11 August 2018 to 21 December 2018 are very small and close to stability, the two monitoring points did not continue monitoring from 21 December 2018 to 16 July 2020).

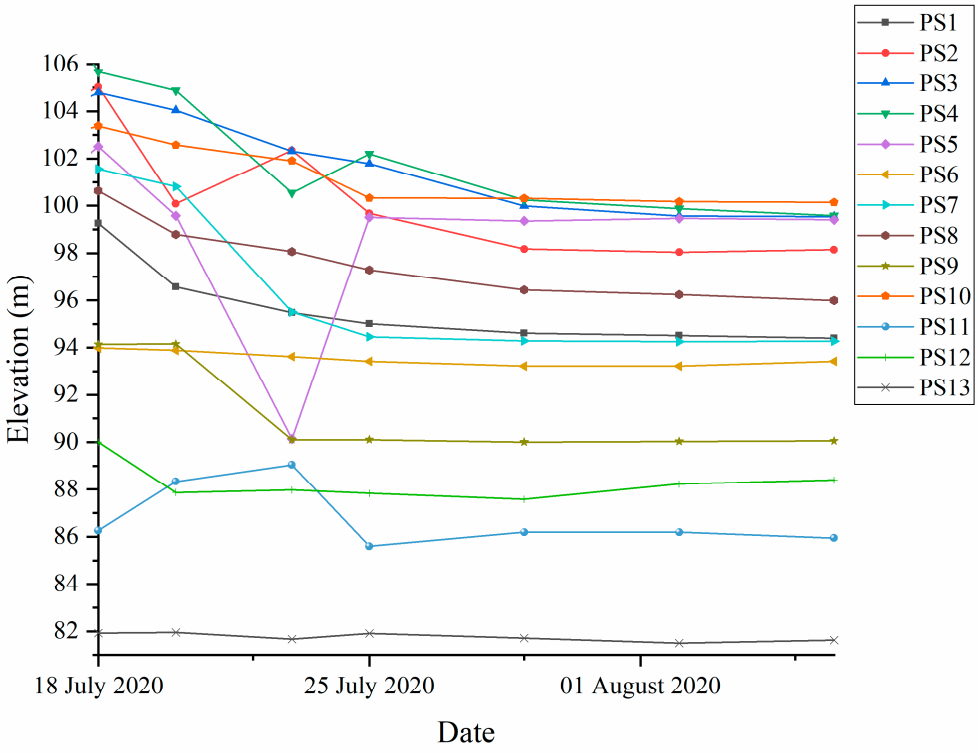

Figure 17. Variation of groundwater level from 18 July 2020 to 9 August 2020. The wellhead elevations of PS1, PS2, PS3, PS4, PS5, PS6, PS7, PS8, PS9, PS10, PS11, PS12 and PS13 are 114 m, 114.5 m, 116.5 m, 117.5 m, 115 m, 104.5 m, 109.5 m, 112 m, 109.5 m, 107 m, 90 m, 95 m and 90 m, respectively.

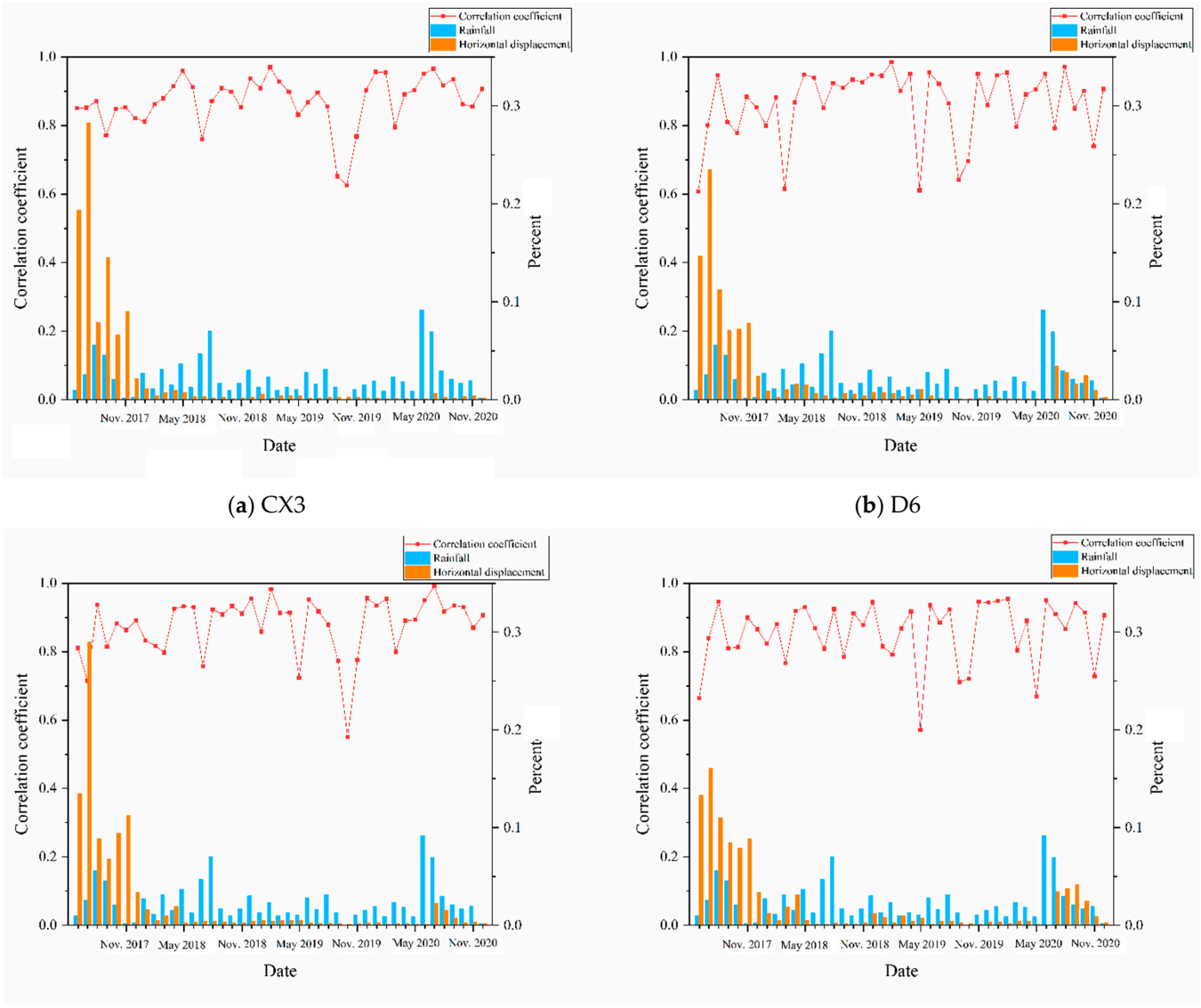

Figure 18. Relationship between rainfall and landslide displacement. The orange histogram represents the ratio of the monthly displacement to the total monitored displacement from 11 June 2016 to 11 December 2022, and the blue histogram represents the ratio of the monthly rainfall to the total accumulated rainfall from 11 June 2016 to 11 December 2022.

It can be also seen that, after landslide reactivation, the influence of the rise in groundwater level on the deep displacement was less than that on the surface displacement. It is worth emphasizing that when the landslide was reactivated, the groundwater level in the landslide was higher than the position of the existing sliding surface. The percentage of the surface vertical displacement of surface monitoring point (D6 and D2) in stage 5 was greater than that of the deep horizontal displacement monitoring points (CX1 and CX3). Moreover, in stage 5, the sliding duration at the surface displacement monitoring points was longer than that at the deep horizontal displacement monitoring points. On points CX1 and CX3, the relatively large deformation lasted one to three months; on points D2 and D6, the relatively large deformation lasted five months. This shows that the deep displacement tended to become stable faster than the surface displacement after the decline in the groundwater level.

3.6. Simulation of Stress Variation after Shallow Soil Landslide

3.6.1. Geological Model

According to the investigation results mentioned before, the geological character profile of the Fangshan landslide can be concluded in Figure 19. There are two sliding surfaces on the profile: one is a soil landslide sliding surface, and the other is rock landslide sliding surface.

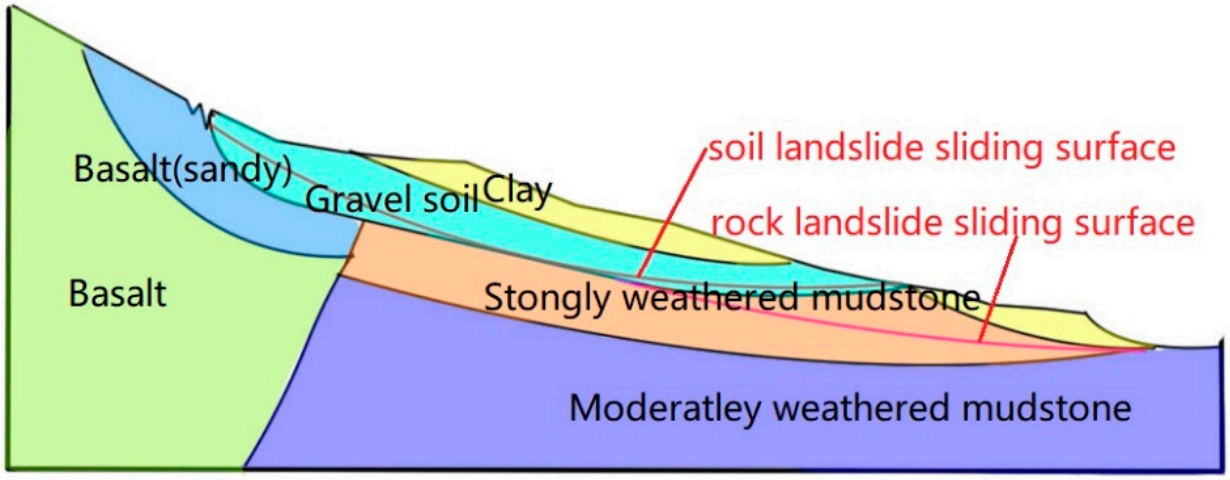

Figure 19. Geological character profile of Fangshan landslide.

3.6.2. Numerical Model

To explore the stress variation on the rock landslide surface, we built the real soil landslide sliding surface in a numerical model (Figure 20), and the stress monitoring point was arranged on the position of rock landslide sliding surface. The length of the model was 198 m, the height on the left side of the model was 75 m, the height on the right side of the model was 19 m, and the width of the model was 1 m. On the model, the length pointing out of the slope was considered the x-axis direction, the vertical height was the z-axis direction, and the width was the y-axis.

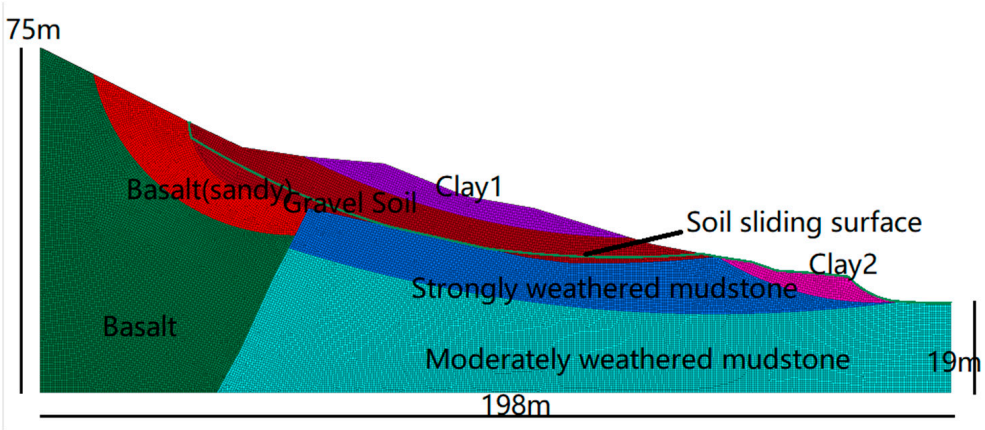

Figure 20. The numerical model of the profile.

3.6.3. Parameter

Combined with the investigation report, the former study and similar landslides occurring nearby, the parameters used in the calculation are shown in Table 2.

Table 2. Parameters of each layer.

Layer	Density (kN/m^3)	Shear Strength		Saturated Shear Strength	
		Cohesion (KPa)	Friction (°)	Cohesion (KPa)	Friction (°)
Clay1	18.6	40	13.6	36	10.6
Gravelly soil	23	10	19.5	7.5	17
Clay2	18.8	45	14	33	9.2
Strongly weathered basalt (sandy)	24	10	35	8	30
Weathered basalt (gravelly)	26.3	100	32	80	25
Strongly weathered mudstone	18.7	36	17.6	30	9.7
Moderately weathered mudstone	24.6	48	17	38	14
Sliding surface		10	19.5	15	6

3.6.4. Calculation Steps

First, the water level line was assigned to the model by means of pore water pressure, and the mechanical parameters were assigned to the corresponding layer. After that, the model was calculated to be stable with the pore water pressure of the low water level (Figure 21a) (the maximum unbalanced ratio was less than 1×10^{-5}), and then the pore water pressure was replaced by the pore water pressure of the high water level (Figure 21b), the corresponding layer parameters were changed, and the model was iterated for 52,000 steps.

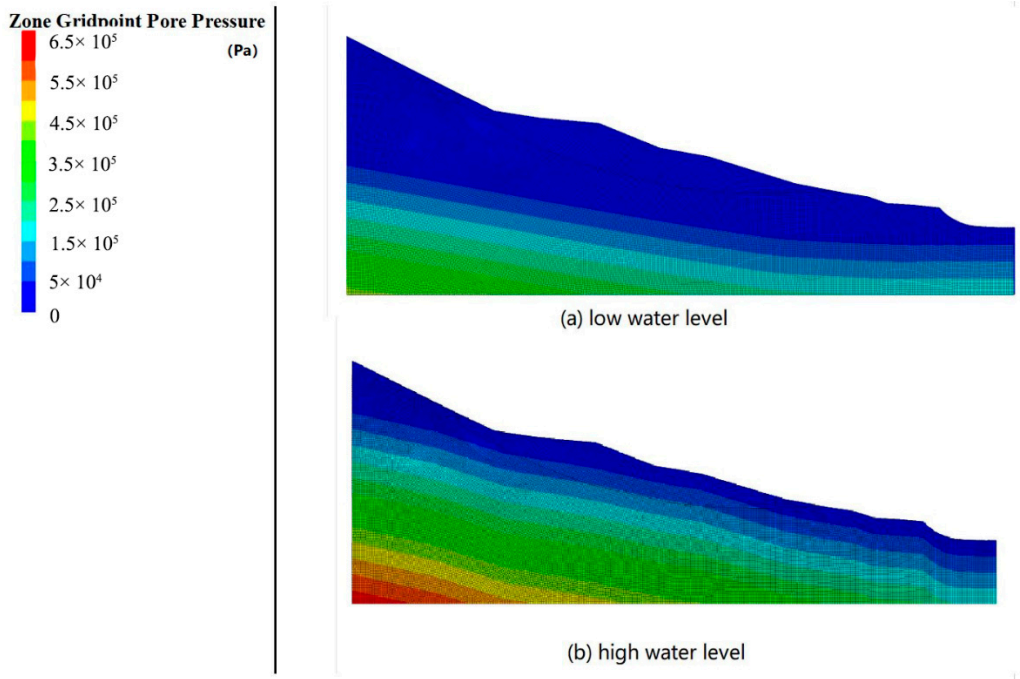

Figure 21. The numerical model of the profile.

3.6.5. Stress Variation

Figure 22 was the result of the calculated displacement, zz direction stress and xx direction stress of the model. To explore the stress variation, we drew Figure 23. Select point A (x: 32.9, y: 0, z: 58.6) on the trailing edge of the landslide to record the displacement, and point B (x: 140.4, y: 0, z: 25.10) to record the stress changes in the zz and xx directions. Take the displacement of point A as the x-axis, and the arithmetic square root of the stress change in the z-direction and xx-direction of point B as the $y1$-axis. Taking the displacement of point A as the x-axis, the ratio of the value of the $y1$-axis to the arithmetic square root of the initial stress in the zz direction and the xx direction of point B was the $y2$-axis. We

found that the stress increase value is 1.29 times the original. The sliding of the overlying landslide did cause a large change in the stress of the underlying layer.

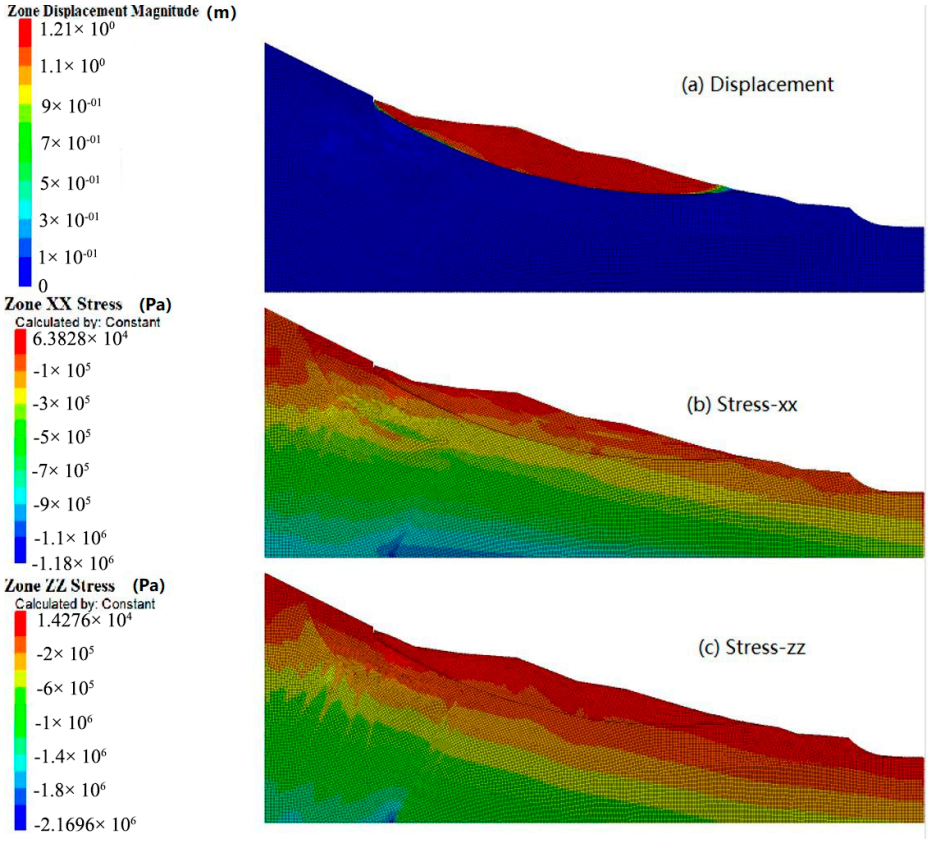

Figure 22. Calculated results of numerical model.

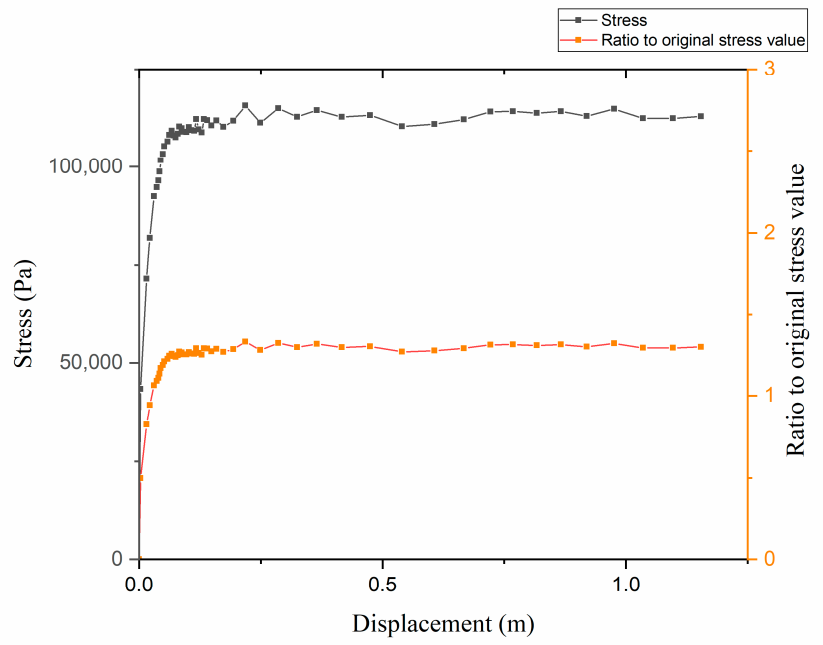

Figure 23. Stress variation after shallow soil landslide. The black line corresponds to the vertical axis of stress on the left, and the orange line corresponds to the vertical axis of the ratio to original stress value on the right.

3.7. Failure Mode of the Fangshan Landslide and Triggering Factors

According to the field investigation and long-term displacement monitoring data, it was concluded that the development stage of the Fangshan landslide was mainly divided into two parts. The first part was the rapid sliding of the shallow soil landslide, and the second part was the creeping of the deep mudstone rock landslide. According to the analysis, the reason for this sequential sliding was probably determined by the unique volcanic stratigraphic structure of the Fangshan scenic area (Figure 18). Due to the influence of volcanic eruptions, the layer at the trailing edge of the landslide was effusive basalt. The layers in the middle part of the landslide from surface to underground were clay layers formed by natural deposits after volcanic eruption, gravel layers formed after basalt weathering after volcanic eruption, and clay and mudstone layers formed before volcanic eruption. The layer at the leading edge of the landslide was clay and mudstone formed by natural deposition. The results of the permeability test show that the layers of gravelly soil, strongly weathered basalt (sandy), and strongly weathered basalt (gravelly) formed after volcanic eruption had a relatively high permeability, and the layers of mudstone and clay formed by natural deposition had a relatively low permeability. During the heavy rainfall season, under a certain rainfall, the gravelly soil layer at the trailing edge of the landslide (region I) became saturated, and the groundwater in the gravelly soil layer changed from phreatic water to confined water with a pressure head because the clay layer was a relative aquiclude. Moreover, the layer at the leading edge of the landslide (region II) was a relative aquiclude, and the groundwater formed by the accumulation from the trailing edge of the landslide and the middle and upper parts of Fangshan Mountain seeped out in the middle of the landslide body (leading edge of region I, Figure 4m). Due to the seepage force formed by the rise of the groundwater and the softening effect on the shear strength of the soil (the change of soil from unsaturated state to saturated state would affect the cohesion and friction of the soil, which would lead to the decrease of soil shear strength) the shallow soil landslide slid along the layer of gravelly soil and the interface between the gravelly soil and strongly weathered mudstone.

When the deep landslide slid (stage 2), the Fangshan landslide was still in a continuous sliding state, and no drainage or other measures were arranged for treatment. According to previous studies, the sliding of the shallow landslide was mainly caused by the rise of water level [16]. Although there was no groundwater level monitoring data at that time, according to the previous field investigations and the movement of shallow landslide, we can expect that the groundwater level must have been at a high level at that time. Due to the sliding of the shallow landslide and rising groundwater level caused by rainfall, the stress in the position of the deep mudstone rock landslide increased greatly. Because of the low permeability of the mudstone layer, it was difficult to drain the water at once. Similar to the shear undrained test, the mudstone was damaged due to the increase in stress. Therefore, the triggering for the deep mudstone rock landslide was due to increased stress caused by the overlaying landslide sliding, the high groundwater level in the landslide and the poor permeability of the mudstone rock layer. According to the monitoring data of the reactivation stage (stage 5) after landslide treatment, the influence of rainfall on surface displacement was much greater than that on deep displacement. In July 2020, due to the failure of drainage wells, continuous rainfall led to the continuous rise in groundwater level around the undrained wells. Under the daily groundwater level, most of the mudstone sliding surfaces were already below the water level, while the surface monitoring points were still above the groundwater level, so the rise of the water level changed the shallow layer from unsaturated to saturated, while the deep layer was always in saturated state. Since the change from saturated state to unsaturated state needs to take a certain time to change, the change of corresponding cohesion and friction also needs time, and because of the influence of surface rainfall, its movement lasted longer than that of the deep sliding surface.

4. Conclusions

This work described a landslide caused by rainfall in a volcanic area. Through field investigation, geophysical exploration by the high-density electrical method and audio-frequency magnetotelluric method, drilling holes, monitoring data, rainfall-displacement correlation analysis results and finite difference simulation method, the geological features and failure mechanisms of this landslide were studied. The following conclusions were drawn:

1. The Fangshan landslide consisted of two parts: a shallow rapidly sliding soil landslide and a deep creep mudstone rock landslide. The failure of the shallow soil landslide triggered the movement of the deep rock landslide.
2. The increased stress in the deep mudstone layer after the overlaying landslide slid and the poor permeability of the mudstone rock layer was the main cause of the deep rock landslide.
3. The displacement deformation trend of the Fangshan landslide was consistent with the rainfall trend. The sensitivity of shallow landslide and deep landslide to groundwater level variation was different, which had a greater impact on the shallow landslide. During the reactivation stage (stage 5), the deep displacement tended to become stable faster than the surface displacement after the decline in the groundwater level.
4. Although the Fangshan landslide had secondary sliding due to the failure of treatment measures, after the water level was dropped by the pumping well, the Fangshan landslide stabilized again. The control measures of active reduction of surface infiltration intensity by arranging plant growth zones and passive reduction of groundwater level by arranging pumping wells at the trailing edge of the landslide have achieved good practice. The Fangshan landslide, the first example of landslide treatment by precipitation pressure in Jiangsu Province, China, provided a good reference for the treatment of similar landslides in engineering practice.

Author Contributions: Investigation resources and validation, W.G. and F.Z.; Writing, W.G. and Z.L.; Conceptualization, F.Z., C.L. (Cheng Lin) and Z.L.; Data curation, Z.L., M.D., Y.L., W.G. and C.L. (Chang Liu). All authors have read and agreed to the published version of the manuscript.

Funding: This research received no external funding.

Conflicts of Interest: The authors declare no conflict of interest.

References

1. Yano, A.; Shinohara, Y.; Tsunetaka, H.; Mizuno, H.; Kubota, T. Distribution of landslides caused by heavy rainfall events and an Chock for earthquake in northern Aso Volcano, Japan from 1955 to 2016. *Geomorphology* **2019**, *327*, 533–541. [CrossRef]
2. Fusco, F.; De Vita, P.; Mirus, B.B.; Baum, R.L.; Allocca, V.; Tufano, R.; Di Clemente, E.; Calcaterra, D. Physically Based Estimation of Rainfall Thresholds Triggering Shallow Landslides in Volcanic Slopes of Southern Italy. *Water* **2019**, *11*, 1915. [CrossRef]
3. Madonia, P.; Cangemi, M.; Olivares, L.; Oliveri, Y.; Speziale, S.; Tommasi, P. Shallow landslide generation at La Fossa cone, Vulcano island (Italy): A multidisciplinary perspective. *Landslides* **2019**, *16*, 921–935. [CrossRef]
4. Prihutama, F.A.; Faruqi, M.D.; Firmansyah, D.N.; Paripurno, E.T. Landslide Hazard Potency Using DEM-SRTM, Landsat 8, and Aerial Photo, Case Study at Ngawen Regency, Gunungkidul District, Yogyakarta. In *International Symposium on Earth Hazard and Disaster Mitigation*; Meilano, I., Cummins, P.R., Zulfakriza, I.T., Eds.; AIP Publishing LLC: Melville, LA, USA, 2018; Volume 1987, ISBN 978-0-7354-1703-8.
5. Uyeturk, C.E.; Huvaj, N.; Bayraktaroglu, H.; Huseyinpasaoglu, M. Geotechnical characteristics of residual soils in rainfall-triggered landslides in Rize, Turkey. *Eng. Geol.* **2019**, *264*, 105318. [CrossRef]
6. Towhata, I.; Goto, S.; Goto, S.; Akima, T.; Tanaka, J.; Uchimura, T.; Wang, G.; Yamaguchi, H.; Aoyama, S. Mechanism and future risk of slope instability induced by extreme rainfall event in Izu Oshima Island, Japan. *Nat. Hazards* **2020**, *105*, 501–530. [CrossRef]
7. Santangelo, N.; Forte, G.; De Falco, M.; Chirico, G.B.; Santo, A. New insights on rainfall triggering flow-like landslides and flash floods in Campania (Southern Italy). *Landslides* **2021**, *18*, 2923–2933. [CrossRef]
8. Belle, P.; Aunay, B.; Lachassagne, P.; Ladouche, B.; Join, J.-L. Control of Tropical Landcover and Soil Properties on Landslides' Aquifer Recharge, Piezometry and Dynamics. *Water* **2018**, *10*, 1491. [CrossRef]
9. Dai, Z.; Zhang, C.; Wang, L.; Fu, Y.; Zhang, Y. Interpreting the influence of rainfall and reservoir water level on a large-scale expansive soil landslide in the Danjiangkou Reservoir region, China. *Eng. Geol.* **2021**, *288*, 106110. [CrossRef]

10. Deng, Q.; Fu, M.; Ren, X.; Liu, F.; Tang, H. Precedent long-term gravitational deformation of large scale landslides in the Three Gorges reservoir area, China. *Eng. Geol.* **2017**, *221*, 170–183. [CrossRef]
11. Kluger, M.O.; Jorat, M.E.; Moon, V.G.; Kreiter, S.; de Lange, W.P.; Mörz, T.; Robertson, T.; Lowe, D.J. Rainfall threshold for initiating effective stress decrease and failure in weathered tephra slopes. *Landslides* **2019**, *17*, 267–281. [CrossRef]
12. Li, Z.; Zhang, F.; Gu, W.; Dong, M. The Niushou landslide in Nanjing City, Jiangsu Province of China: A slow-moving landslide triggered by rainfall. *Landslides* **2020**, *17*, 2603–2617. [CrossRef]
13. Xia, M.; Ren, G.M.; Yang, X.L. Mechanism of a catastrophic landslide occurred on May 12, 2019, Qinghai Province, China. *Landslides* **2020**, *18*, 707–720. [CrossRef]
14. Setiawan, H.; Wilopo, W.; Wiyoso, T.; Fathani, T.F.; Karnawati, D. Investigation and numerical simulation of the 22 February 2018 landslide-triggered long-traveling debris flow at Pasir Panjang Village, Brebes Regency of Central Java, Indonesia. *Landslides* **2019**, *16*, 2219–2232. [CrossRef]
15. Tohari, A.; Wibawa, S.; Koizumi, K.; Oda, K.; Komatsu, M. Effectiveness of siphon drainage method for landslide stabilization in a tropical volcanic hillslope: A case study of Cibitung Landslide, West Java, Indonesia. *Bull. Eng. Geol. Environ.* **2021**, *80*, 2101–2116. [CrossRef]
16. Yu, L.; Yan, C.; Guo, S.; Tan, J.; Guo, J.; Lou, Z.; Wan, J. Analysis of the mechanism and failure mode of landslides subjected to transient seepage in a Piedmont region of Nanjing area. *Bull. Eng. Geol. Environ.* **2021**, *80*, 7441–7456. [CrossRef]
17. Jing, F.; Wang, Y. Analysis of water and rain information on "July2016" torrential rain in Nanjing. *Jiangsu Water Resour.* **2016**, *22*, 39–41. [CrossRef]